Self-Assembly of Nucleoside-Derived Low-Molecular-Weight Gelators: A Thermodynamics and Kinetics Study on Different Length Scales

Omar El Hamoui, Karen Gaudin, Serge Battu, Philippe Barthélémy, Gaetane Lespes, Bruno Alies

Self-assembly of Nucleoside-derivatives Low Molecular Weight Gelators: A Thermodynamics and Kinetic study at different length scales

Omar El Hamoui,[1,2] *Karen Gaudin,*[1] *Serge Battu,*[3] *Philippe Barthélémy,*[1] *Gaëtane Lespes,**[2] *Bruno Alies*[*,1].

1. Université de Bordeaux, INSERM U1212, UMR CNRS 5320, F-33076 Bordeaux, France

2. Université de Pau et des Pays de l'Adour (E2S/UPPA) CNRS, Institut des Sciences Analytiques et de Physico-Chimie pour l'Environnement et les Matériaux (IPREM), UMR 5254, 2 Avenue Pierre Angot, 64053 Pau Cedex, France

3. EA3842- CAPTuR, GEIST, Faculté de Médecine, Université de Limoges, 2 rue du Dr Marcland, 87025 Limoges Cedex, France

Keywords: Low Molecular Weight Gelators, LMWG, Nucleosides-derivatives, Self-assembly, Hydrogel

Abstract. Biocompatible materials are of paramount importance in numerous fields. Unlike chemically-bridge polymer-based hydrogels, low molecular weight gelators can form a reversible hydrogel as their structure rely on non-covalent interaction. Although many applications with this type of hydrogels can be envisioned, we still lack their understanding due

to the complexity of their self-assembly process and the difficulty predicting their behaviors (transition temperature, gelation kinetic, impact of solvent…). In this study, we extend the investigations of a series of nucleoside-derivatives gelators which only differ by subtle chemical modifications. Using a multi-technique approach, we determined their thermodynamic and kinetic features at various scale (molecular to macro) in different conditions. Monitored at supramolecular level by circular dichroism as well as macroscopic scales by rheology and turbidimetry, we found out that sol-gel and gel-sol transition are greatly depending on the concentration and on the mechanisms that are probed. Self-assembly kinetic depends on hydrogel molecules and is modulated by temperature and solvent. This fundamental study provides insight on the impact of some parameters on the gelation process, such as concentration, cooling rate and nature of the solvent.

Introduction

Low Molecular Weight Gelators (LMWG) have been of particular interest for the last decades, since they have the ability to self-assemble into fibrillar structures. The fibers entangled themselves, creating a network arrangement that entraps the solvent. This system forms a soft viscoelastic supramolecular gel[1–3]. LMWG hydrogelation features have potential applications in life science fields, *e.g.* tissue engineering[4–6], cell culture[7–10], drug delivery[11,12], alongside polymer gels. Polymer gels are formed primarily by covalent interactions between monomers, whereas supramolecular gels consist of self-assembling of the building blocks by weak interaction (hydrogen bonds, Van Der Waals interactions, π-stacking…). This particular characteristic gives advantages compared to polymer gels, like among others the thermo-reversibility of the gelation process. To match these properties, designing amphiphilic molecules

has shown to be an efficient strategy since these kinds of molecules tend to spontaneously self-interact in aqueous media, by a balance of hydrophobic and hydrophilic interactions. To this day, plenty of examples of successful LMWG design are listed and imply peptides[13–17], nucleobases[18–20], urea and amide based molecules[21], and versatile derivatives[22–29]. Despite the apparent well-known features that characterize supramolecular gels, the hydrogelation process remains poorly understood. At this point, the approach to find a hydrogelator candidate is empirical and rationalizing the strategy of LMWG design is still a challenge[30,31]. LMWG studies face lot of other issues, among them are the versatility and the reproducibility of the results, needing the parameters impacting them to be caught and mastered. These kind of issues were recently addressed and illustrated with examples of peptide-based LMWG triggered and affected by the pH, where the parameters influencing the gelation (temperature, physicochemical properties of the medium…) were discussed, as well as the different techniques that can be mobilized at every scales to study them[32]. Differences in the properties of this type of gels were observed from macroscopic visual aspects to molecular assembly level, by tuning the properties of the medium[32–34]. Although, the fact is that the demand of more exhaustive information about what could influence the gelation process is still a recent issue in the field of LMWG[35]. Because supramolecular gels are in a metastable state that result from thermodynamic and kinetic processes[36], this field required more of their studies in order to get crucial insights on gelation process[37]. Some recent studies were undertaken in that way, by probing for example the gelation process and kinetic in terms of rheological behavior and supramolecular features, using a pool of different techniques[38]. Others focused on the use of computational methods in order to predict the gelation process features, that can indeed be of great help combined with experimental data to facilitate the design of LMWG and to bring more light on the fundamental aspect of the

gelation mechanism[39]. Still, to complete the state of art in a more integrated view, the great diversity of LMWG molecular nature requires the same diversity of studies. In order to seek in this direction, we focus on specific types of LMWG: glyco-nucleo-bolaamphiphiles (GNB). GNB are bioinspired amphiphilic molecules as they are made of nucleosides and lipids. Bola-amphiphiles general molecular structures have already shown their self-assembling properties because of their ability to balance well hydrophobic and hydrophilic interactions[40], so GNB benefit of these advantages to successfully form a gel. They also display a low toxicity and have been used *in vivo*[28]. The molecular architecture of these GNB consists of two glyco-modified thymidines linked by a hydrophobic segment and triazole moieties (**Figure 1**).

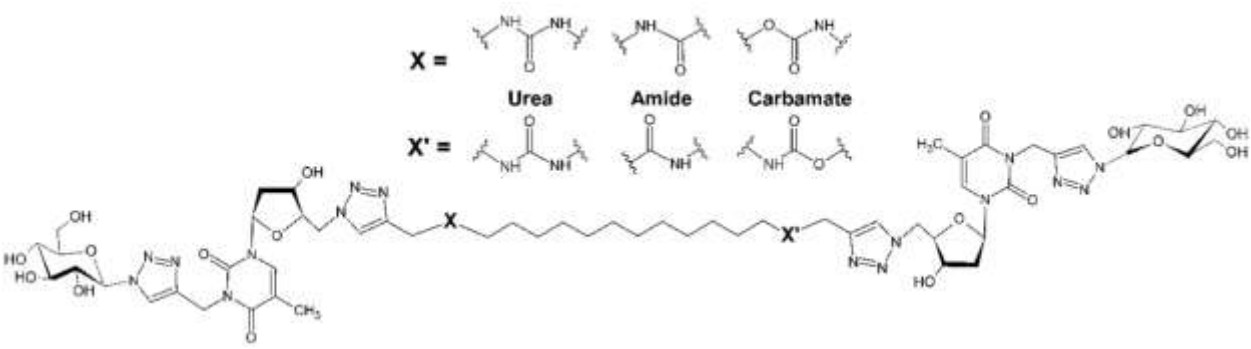

Figure 1: Chemical structure of molecules studied named Glyco-Nucleo-Bola-Amphiphiles (GNB). Abbreviations of molecules are BU when X = X' = urea; BA when X = X' = amide and BC when X = X' = carbamate.

GNB-based hydrogels form a network with solvent trapped into the mesh as shown by cryo-SEM experiments (**Figure 2**). It is important to note that despite the ability of cryo-SEM to keep sample in its native state as much as possible, alterations of the sample cannot be ruled out. GNB structures that are studied here differ only by the nature of the linker between the glyco-

nucleoside and the aliphatic parts of the molecule. In **Figure 1**, we show the three different GNB we investigated, with a linker made of urea (BU), amide (BA) or carbamate (BC). Even though they all have gelating properties with a relatively same mesoscopic architecture, they exhibit different thermal, kinetic and rheological properties. Previous study showed the involvement of additional hydrogen-bonding sites contributing to higher elastic modulus G' and gel-sol transition temperature[28]. Interestingly, they all tend to form a gel at room temperature, after solubilization by heating cycle, except BC that has to be stored at low temperature (< 10 °C) in order to form a gel homogeneously[26]. In this study, we aim to explore specific aspects: their thermal and structural properties. The results that are presented here are another contribution for sparking debate over the relationship between kinetic and thermodynamic in the gelation process, especially the time-temperature dependency in the process of homogeneous nucleation and fibers growth that lead to the gel phase. Issues about technical limitations for the study of these kinds of materials, as well as the relevancy of some methods, are also addressed and discussed.

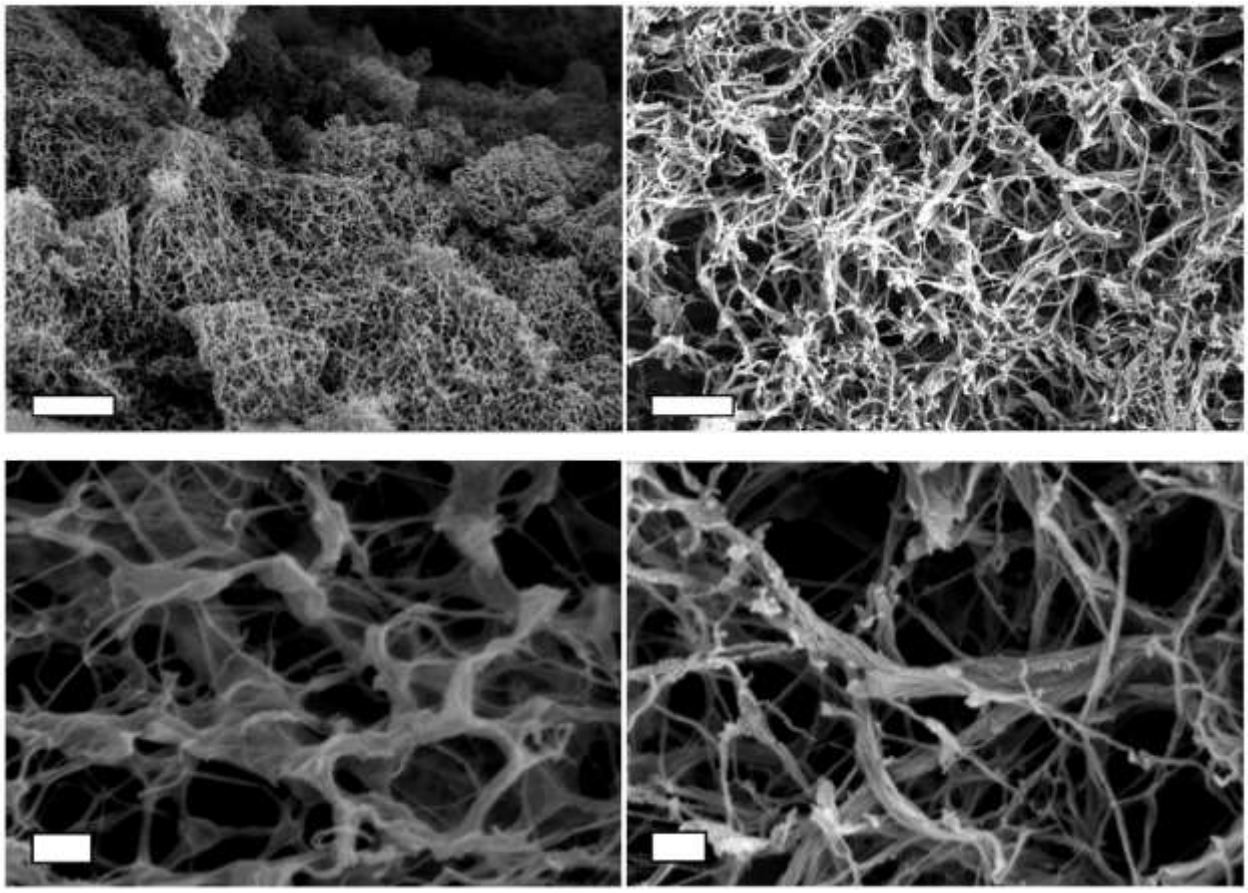

Figure 2. Scanning cryo-electron micrographs. BU (left panels) and BA (right panels) at two magnifications, scale bar = 1μm (top panels) or 200nm (bottom panels). Condition: 1% w/v prepared in PBS.

Materials & Methods

Sample preparation

Gels at 1% and 2% w/v were formed by weighting the aimed amount of GNB powders (10 mg and 20 mg, respectively) and adding the right volume of solvent (1 mL of ultrapure water or PBS). GNB used were synthesized in-house accordingly by previous procedures[26,28]. The

mixtures were sonicated for 30 seconds, heated at 82 °C (this temperature was arbitrary selected in order to solubilize our samples) for 10 min to ensure complete solubilization, then they remained at room temperature for gelation to occur (4 °C for BC). All gels below 1% w/v were obtained by successive dilutions of solubilized 1% w/v or 2% w/v preparations. Ultrapure water used was deionized water with resistivity of 18.2 MΩ. Dulbecco's Phosphate Buffer Saline (PBS) (without magnesium and calcium) was purchased from Sigma Aldrich.

Cryo-scanning electron microscopy (cryo-SEM)

Cryo-SEM microscopy experiments were conducted on a ZEISS GEMINI 300 at Bordeaux Imaging Center (BIC). The samples were cryo-fixed by high pressure freezing with a LEICA EM-HPM100. Cryo-SEM micrographs were obtained after sublimation (26 min for BU and 30 min for BA) and 30 s of sample platinum metallization.

Rheology experiments

Rheological measurements were carried out on a Malvern Kinexus Pro+rheometer with steel cone-plate geometry (diameter: 20 mm). The lower plate is equipped with a Peltier temperature control system. A solvent trap was used to ensure homogeneous temperature and to prevent water evaporation. BU, BA and BC 1% w/v in PBS were heated at 85 °C and the resulting solution was deposed on the motionless disk of the rheometer, then cone-plate was set and the gel could rest and cure between the disks. Frequency sweeps were performed at 25 ± 0.01 °C for BU and BA and 10 °C ± 0.01 °C for BC within the linear viscoelastic regime (LVER) at a strain of 0.1% to access the rheological moduli in a first place. Moduli were taken at a frequency of 1 Hz (ω = 6.283 rad s^{-1}). Temperature sweeps were conducted at 5 angular frequencies (3.149,

6.283, 19.87, 31.49 and 62.83 rad s^{-1}), in controlled stress condition (3 Pa) and in another run in controlled strain amplitude condition (0.1 %) in order to compare the effect of mechanical stress on gel-sol and sol-gel transition temperatures, on a range of temperature depending on the hydrogelator conditions (25-85 °C for BU and BA, 4-40 °C for BC) and with a temperature ramp of 2 °C min^{-1}. To characterize the gel-sol transition, frequency sweeps were done on a range of temperature near the expected gel-sol region of each gel and the gel point was approximated at the temperature region where the moduli are proportional to a power law of the frequency, based on Winter's criterion[41]. Gelation kinetic was performed for BC by deposing the melted solution into the rheometer and measuring G' and G'' as a function of time every minute at 4 °C, at the same 5 angular frequencies as taken for temperature sweeps experiments, and with a controlled strain amplitude of 0.1%.

Turbidimetry

Turbidity measurements were performed on a Perkin-Elmer UV-vis spectrometer (Lambda 25) coupled with a Peltier device (PTP 6). Hydrogels initially prepared at the aimed concentration for the purpose of the experiment were heated at 82 °C for at least 5 minutes to ensure complete solubilization then poured into quartz UV cuvette (optical path length: 1 cm). Absorbance at 500 nm was measured as an indicator of turbidity with a time interval of 1 minute for the temperature scans and 2 minutes for the gelation kinetic of BC. For the temperature scan measurements, three cycles of heating and cooling were done with a ramp of 1°C min^{-1}, on a temperature range depending on the hydrogelator conditions (20-85°C for BU, 10-70°C for BA and 1-64 °C for BC).

Differential scanning calorimetry

Differential Scanning Calorimetry (DSC) was realized using METTLER TOLEDO. A total of two to three heating and cooling cycles were performed, on a range of temperature depending on the hydrogelator condition (27-87 °C for BU, 15-75 °C for BA) at 1% and 2% w/v in ultrapure water or in PBS at a constant rate of 1, 2 and 5 °C min^{-1}, in 100 µL aluminum crucibles. Heating cycle for BC 1% and 2% w/v in ultrapure water or in PBS was preceded by a waiting time of 30 min at 2 °C to ensure gelation, then was conducted at a ramp of 1 and 2 °C min^{-1} from 4 to 61 °C. Heat flow was also measured as a function of time for BC in isothermal condition at 4 °C after solubilization at 60 °C. Heating and cooling results of thermal analysis are reported in Table 1. These experiments were independently replicated at least two times. Mean values and standard deviation values are extracted from the replications of at least two temperature cycles per run.

Circular Dichroism /UV-Vis spectroscopy

UV-Vis and Circular Dichroism (CD) spectroscopy were performed on JASCO J-1500 Circular Dichroism (optical path length = 0.2 cm) in quartz cuvette coupled with a Peltier device. Spectra were acquired at 82 °C to ensure complete solubilization for the disassembled hydrogelators and at 4 °C and 25 °C for the self-structured BC and BU/BA respectively, at 0.05% w/v in pure water and PBS. Temperature scans were done on a range of temperatures depending on the hydrogelator conditions (10-80 °C for BU, 10-75 °C for BA and 5-60 °C for BC), by acquiring spectra each 5 °C step in heating and cooling paths. BA was systematically solubilized between each acquisition during cooling to avoid aggregate formation. Scan interval was assessed for BC by acquiring spectra each 5 minutes at 4 °C after solubilization at 60 °C.

Thermal denaturation cycles were done by monitoring at one wavelength (268 nm for BU, 230 nm for BA, 276 nm for BC; corresponding to their self-assembled spectrum) every 1 °C at a temperature rate of 1 °C min^{-1}, in heating and cooling ways. Van't Hoff analysis was then done on these data. Kinetic of BC was performed by monitoring at one wavelength in CD every minute at 4°C after solubilizing at 60 °C.

Results and discussion

To get insight on the self-assembly process leading to hydrogels, we compared conformational and thermal properties of these gelators (BU, BA, BC, see **Figure 1**) between two media, water and PBS, at different scales (from molecular to macroscopic gel) and different concentrations. We used different techniques to relate several features of the gels to their intrinsic properties: temperature-monitored turbidimetry was done based on the visual turbid aspect of the GNB in gel phase that is lost in solution phase to access the thermal phase transition and kinetic data; differential scanning calorimetry (DSC) and sol-gel rheometry were done in order to relate the thermal stabilities and optical features of the gels in terms of heat exchanges and mechanical properties; circular dichroism (CD) and UV-vis spectroscopy were assessed to relate thermal and kinetic properties of these GNB to the conformational properties at the self-assembly scale using induced supramolecular chirality upon self-organization.

1. Phase transition of GNB

    1.1.Rheometry

Rheometry measurement was done in a purpose of mechanical based characterization of the temperature-state relationship of these hydrogelators. As it was previously determined[26,28] the kind of linker moiety of the GNB impacts its rheological properties. Frequency sweep experiments with a constant strain amplitude of 0.1% show a storage modulus G' of 52.4 (± 12.7), 4.0 (± 2.0) and 1.0 (± 0.6) kPa for BU, BA and BC 1% w/v in PBS, respectively (**Figure 3**).

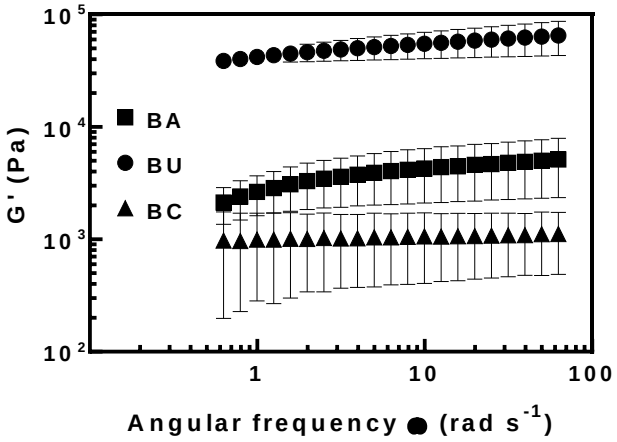

Figure 3. Frequency sweep experiments. G' function of frequency with BU (circle), BA (square), BC (triangle) in PBS. Error bars represent standard deviation based on three independent gel preparations. Condition: [GNB] = 1% w/v.

Although mechanical properties arise out of global fibrillar architecture of the supramolecular gel, they are also strongly influenced by the design of the molecule structure. The greater G' of BU may come from the multiple fiber branching constituting its network, compared to the BA that has fiber joints instead (**Figure 2**), but also from the urea group that provides additional oriented hydrogen-bond sites and thus stronger intermolecular interaction[28]. The linker has also an impact on the thermal stability based on gel-sol transition experiment.

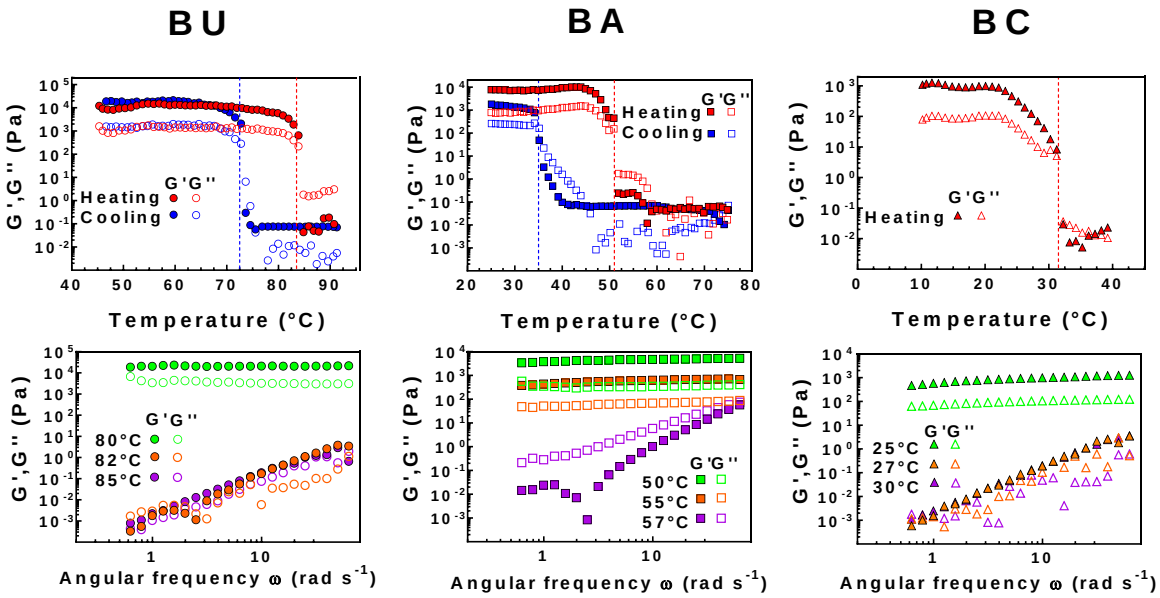

Figure 4. Gel-sol experiments. G' (full symbols) and G'' (open symbols) function of temperature (top panels) in heating (red) or cooling (blue) with BU (left panel, circle symbols), BA (middle, square symbols) and BC (right, triangle symbols) and their frequency sweeps (bottom panels) at three temperatures (green, orange or purple) near the gel-sol transition. Dashed lines represent expected regions of transition, at the crossover point of G' and G''. Condition: [GNB] =1% w/v in PBS at an angular frequency of 6.283 rad s^{-1} in a controlled stress of 3 Pa. Rate of heating/cooling= 2 °C min^{-1}.

G' and G'' function of temperature with BU, BA and BC experiments are presented in **Figure 4 top panels**. Heating cycles show a region where the moduli dramatically drop, around 82 °C, 52 °C and 30 °C for BU, BA and BC respectively. To determine the gel-sol transition, according to the Winter and Chambon method[41,42], frequency sweeps were done at different temperatures around the G'-G'' crossover observed in the temperature sweep graphs (**Figure 4 bottom panels**). In the gel phase, the moduli do not depend on the frequency, over the range of

angular frequencies of the experiment. When the gel-sol transition occurs, the moduli follow a power law dependency on the angular frequency ($G' \sim G'' \sim \omega^n$). At 55 °C, BA remains in gel phase owing to the moduli independent of the frequency, but exhibits a liquid-like behavior at 57 °C as $G' < G''$, $G' \sim \omega^2$ and $G'' \sim \omega$, meaning that the gel-sol transition is near this region of temperature[42]. BU and BC remain in gel phase at 80 °C and 25 °C respectively but the transition to the sol phase does not exhibit the same power laws. BU seems to turn into sol phase at 82 °C with G' and G'' being proportional to ω^2 and ω, although at 85 °C the moduli become $G' \approx G'' \sim \omega^{1.8}$. For BC at 30 °C, $G' \sim \omega^{1.8}$ and $G'' \sim \omega^{1.2}$, which is a characteristic close to a viscous fluid, and at 27 °C the G' and G'' follow intermediate power laws, $\omega^{1.9}$ and $\omega^{1.6}$, respectively. No others intermediate power laws were found in the range of temperatures of the experiment.

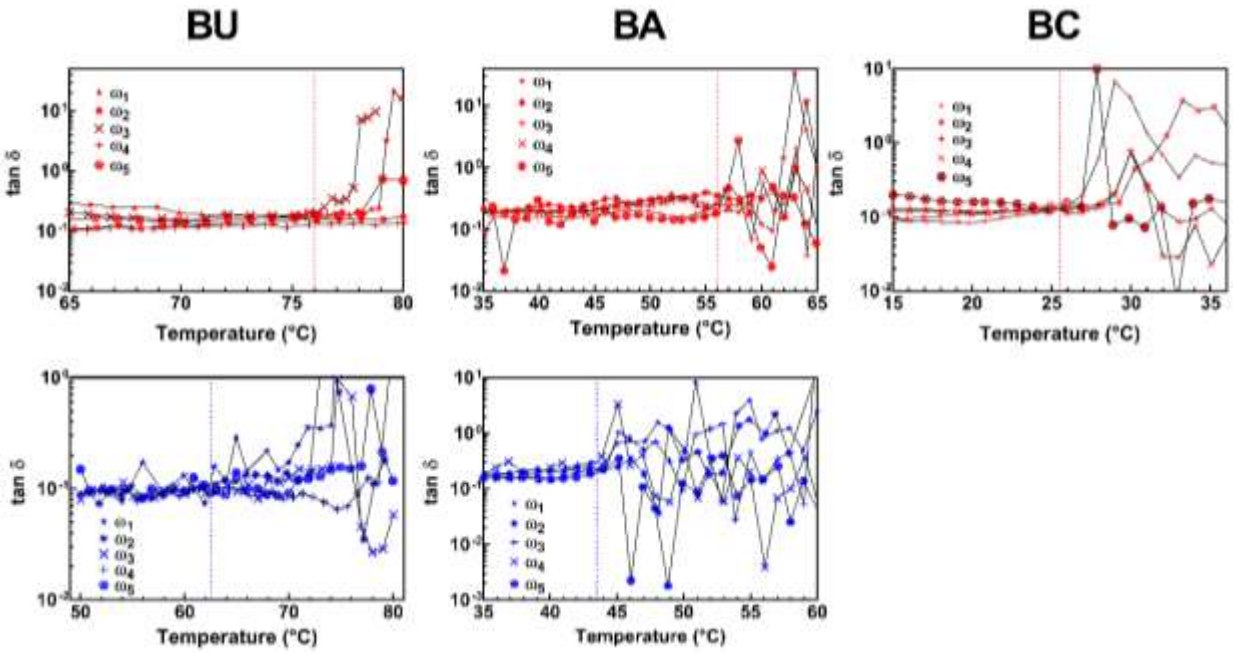

Figure 5. Determination of the gel-sol and sol-gel transition temperature by the tan δ method, in heating (top) and cooling cycle (bottom). Dotted lines indicate the estimated temperature of transition. ω_1 to ω_5 are equals respectively to 3.149, 6.283, 19.87, 31.49 and 62.83 rad s^{-1}.

Another way to determine transition temperature consists on taking the convergence point of tan δ-temperature plots of a pool of different angular frequencies, where tan δ = G'' / G'. Here, a clear convergence point was not shown by these plots, but instead a point separating two regions, one where tan δ is quite stable with a value around 0.1, and another where it is more erratic and divergent. This permits a rough approximation of the temperature of gel-sol transition of each GNB, being 76 °C, 56 °C and 25.5 °C for BU, BA and BC respectively (**Figure 5 top panels**). These temperatures will be then referred as $T_{gel\text{-}sol}$. These values are consistent with the power law behaviors previously observed (**Figure 4 bottom panels**) and with temperature sweep experiments at different frequencies that are reported in ESI (**Figure S13-S17**). This concordance between different ways to access the phase transition was previously reported in other works on thermally triggered and ionic gels[43,44], but as their authors have acknowledged, and for the sake of rigorous definition, the point of G' and G'' drop in values in temperature sweep experiment will be then referred as G'-G'' crossover point.

A cooling cycle was done for BU and BA just after their heating cycle to further investigate their gelation upon cooling. It showed a sharp recovery of its initial G' at a temperature of G'-G" crossover point below $T_{gel\text{-}sol}$ in some conditions (**Figure 4 top left and top middle panels**). Temperature of sol-gel transition could be extracted from the tan δ plots of cooling cycles for BU and BA, being respectively 62.5 °C and 43.5 °C (**Figure 5 bottom panels**). These temperatures, also consistent with the G'-G'' crossover point upon cooling, will be then referred as $T_{sol\text{-}gel}$. No $T_{sol\text{-}gel}$ was determined for BC since it does not form a gel upon a cooling sweep.

These profiles of G' and G'' upon heating and cooling with this kind of hysteresis were previously observed with other LMWG and explained by the fact that the heating triggers a

progressive dissolution of the gels, shown by the progressive decrease of the moduli. Whereas during cooling, even if LMWG nuclei can be formed, the gel properties are recovered once the network has expanded in the whole sample volume, shown by the sharp increase of the moduli[45]. Noteworthy that there are some differences whether the stress or the strain amplitude was chosen to be controlled. For example, BA does not cure upon cooling in controlled stress condition above 6.283 rad s^{-1}, but does in controlled strain amplitude (**Figure S15-16**). G'-G'' crossover point on the heating plots of BA varies between controlled stress and strain conditions, with values around 50 °C and around 60 °C for controlled stress and controlled strain amplitude respectively, showing the dependency of the transition on the parameters of the experiment that are impacting the sample (**Table S1**). Previous work showed that gelation of BC occurs at low temperature (< 10 °C)[26]. Gelation kinetic was performed at 4 °C by measuring the G' and G'' every 30 seconds at the same 5 frequencies chosen in temperature sweep experiments and a constant strain amplitude of 0.1% (**Figure 6 top**, **Figure S18**). The gel point determination of BC was attempted by the Winter and Chambon method[41,42], consisting on taking the crossing point of the tan δ of different frequency plots. The gel point was roughly determined by taking the point of stabilization of the tan δ of each frequency, which falls at 9 min and 30 s. The moduli kept around zero during a whole induction time stage, then began a linear growth stage of the gelation process at a t_{gel} = 4.5 min, after which the moduli started to increase. The G' becomes ten times greater than the G'' after the gel point and reaches a pseudo-equilibrium after 20 min where the gelation enters in a non-linear growth stage. All the gelation kinetic plots at each frequency are reported in ESI (**Figure S18**). To describe more deeply the linear growth stage, an Avrami model[46] of this stage was used. This model describes well the nucleation-

growth kinetic of fractal objects, particularly crystals[47–49], and has been applied to gels since they involve similar mechanisms[50,51]. The model has this general form

$$\ln(1 - X) = -K(t - \tau)^{n_A}$$

(eq. 1.1)

where K is a constant related to the rate of growth, t is time, X the volume fraction of self-assemblies, n_A the Avrami exponent and τ the induction time of self-assembling. The Avrami exponent denotes the dimension of the self-assemblies forming the gel, which is equal to 1, 2 or 3 for 1-D, 2-D or 3-D dimensional growth respectively. The induction time here is approximated as t_{gel}. X is expressed in terms of the storage modulus G' as following

$$X = \frac{G'(t) - G'(0)}{G'(\infty) - G'(0)}$$

(eq. 1.2)

The plots in **Figure 6 bottom** is derived from the model by integrating (eq. 1.2) into (eq. 1.1) and taking the natural logarithms. The slope corresponds then to n_A which is here equal to 1.4 ± 0.2, which is in accordance with a one-dimensional fiber growth with very few branching[50]. This result matches well with previous works that also describe the dimensionality of the growth of supramolecular gels, where the kinetic properties of the gel growth and the microscopic features of the gels that are observed in microscopy experiments are well related.[51]

These results show that the fine molecular design impacts the rheological aspect of the hydrogels, in terms of viscoelasticity and phase-transition temperature. Moreover, these transitions have different kinetic scale. BU and BA form a gel relatively fast upon cooling compared to BC when they reach their sol-gel transition temperature. Taking into consideration these timescales, the gelation of BU and BA is considered as a non-isothermal process, whereas

BC is formed by an isothermal gelation, which fits well an Avrami kinetic model (corresponding to 1-Dimensional growth).

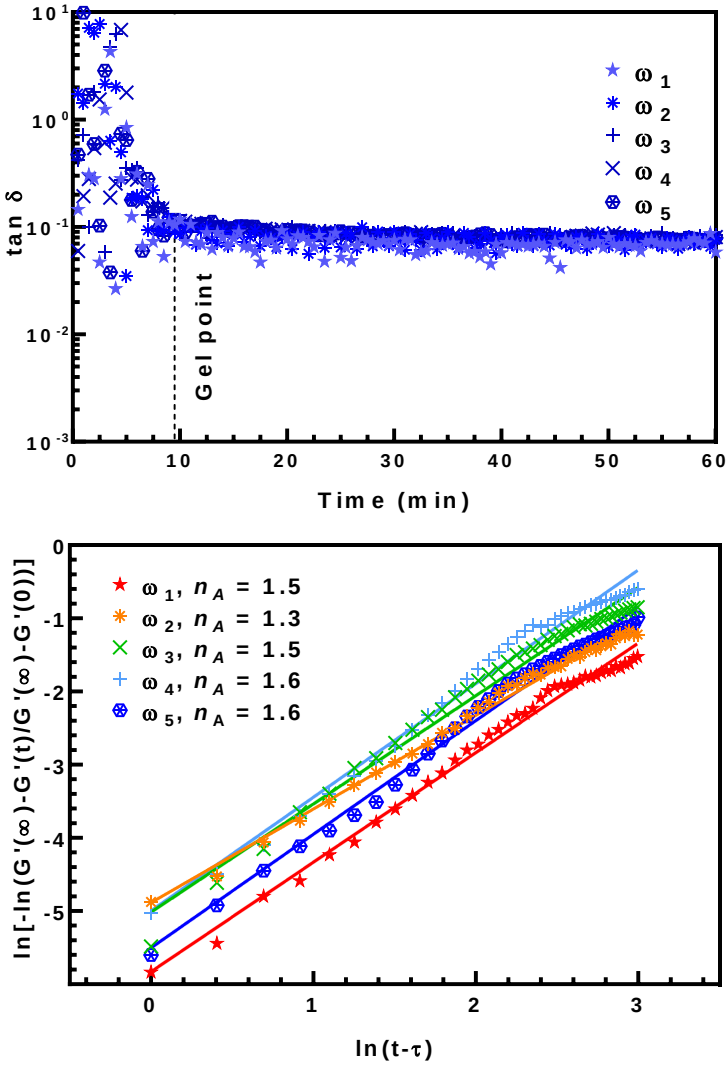

Figure 6. Kinetic features of BC. Gel point determination of BC (top panel) and Avrami plot (bottom panel). Condition: [BC] = 1% w/v in PBS at 4 °C. ω_1 to ω_5 are equals respectively to 3.149, 6.283, 19.87, 31.49 and 62.83 rad s^{-1}.

1.2. Turbidimetry

Turbidimetry can be used to monitor gel visual aspect to go further in the thermal and kinetic properties of those gels. Indeed, these molecules form a turbid gel and a transparent sol phase when completely solubilized. This technique can probe at an early stage of the gelation process the first self-assembled objects that can scatter light. In order to determine phase-transitions temperature, we measure absorbance at 500 nm as function of temperature (**Figure 7**). No significant difference was observed in transition temperatures between water and PBS conditions (see also **Figure S10-12**). Interestingly, heating and cooling cycles exhibit a thermal hysteresis. Heating cycles show a melting temperature T_m of 80 °C and 60 °C for BU and BA gelators, respectively. Their hysteresis is quite high ($\Delta T \approx 20$ °C), and during cooling, once a cooling temperature T_c is reached, the gelation seems to occur quite fast, with a big leap in turbidity at 60 °C and 40 °C for BU and BA respectively. These observations match with rheometry experiments, where the $T_{gel-sol}$ corresponds to the T_m, although the $T_{sol-gel}$ can slightly differ from the T_c. It is important to note that from rheology experiment, the explanation that could be given to the hysteresis was based on the mechanical properties of the gel that are recovered once the network has expanded in the whole volume, even if nuclei were formed while the sample is cooling. The fact is that turbidimetry shows no scattering effect from the formation of objects during the whole time of the hysteresis (20 min). This indicates that nucleation seems to be triggered only once the sample cooled to T_c and it starts to spread at that moment. As in rheometry experiments, the BU and BA gelation is non-isothermal. Differences in sol to gel transition could be explained by the stress and strain conditions under the cone-plate geometry that influence the gelation process and the fibers orientation and organization during temperature ramp. Also, temperatures ramps were not the same (1 °C min^{-1} for turbidimetry, 2 °C min^{-1} for

rheology) and these techniques do not monitor the same feature. Since turbidity is not directly related to elastic deformation some differences can be observed. BC has also a thermal hysteresis but its gel formation does not occur at the same rate as the two others upon cooling. To determine the T_c, turbidity was measured in isothermal conditions as a function of time at different low temperatures (**Figure 8**).

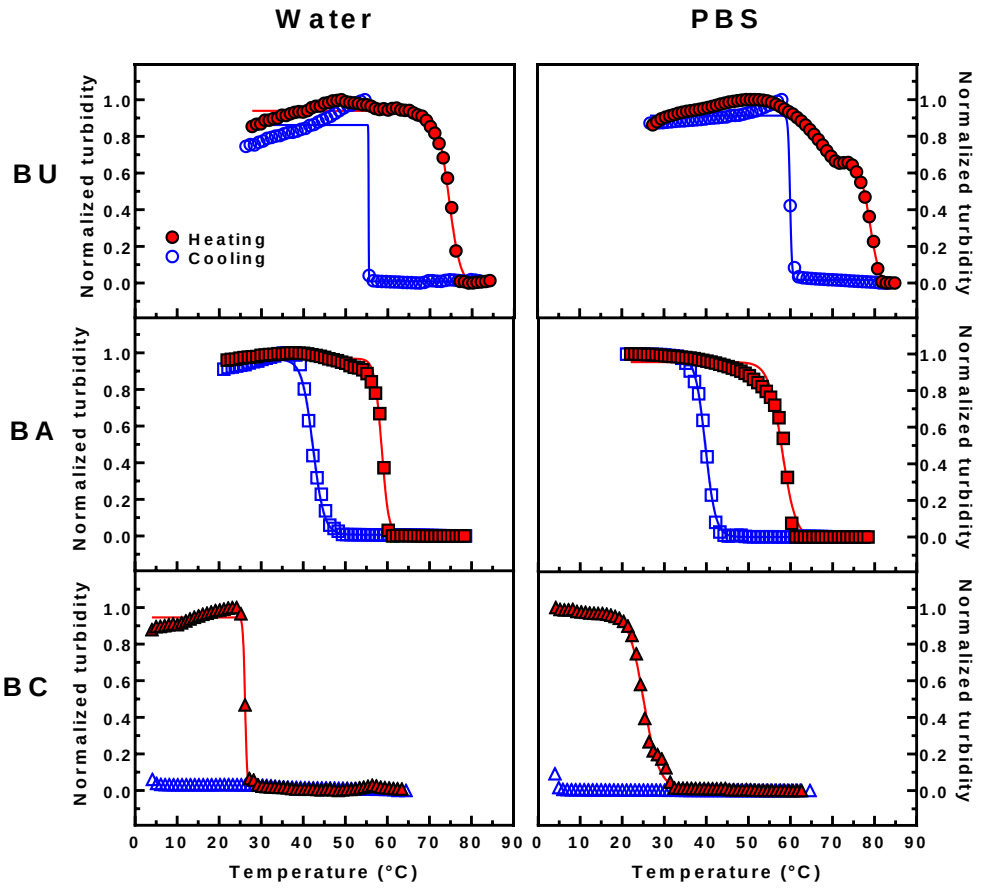

Figure 7. Turbidimetry of BU (top), BA (middle), BC (bottom) during heating (red full symbols) and cooling cycles (blue open symbols) in water (left) or PBS (right). Condition: [GNB] = 1% w/v. Temperature ramp: 1 °C min^{-1}.

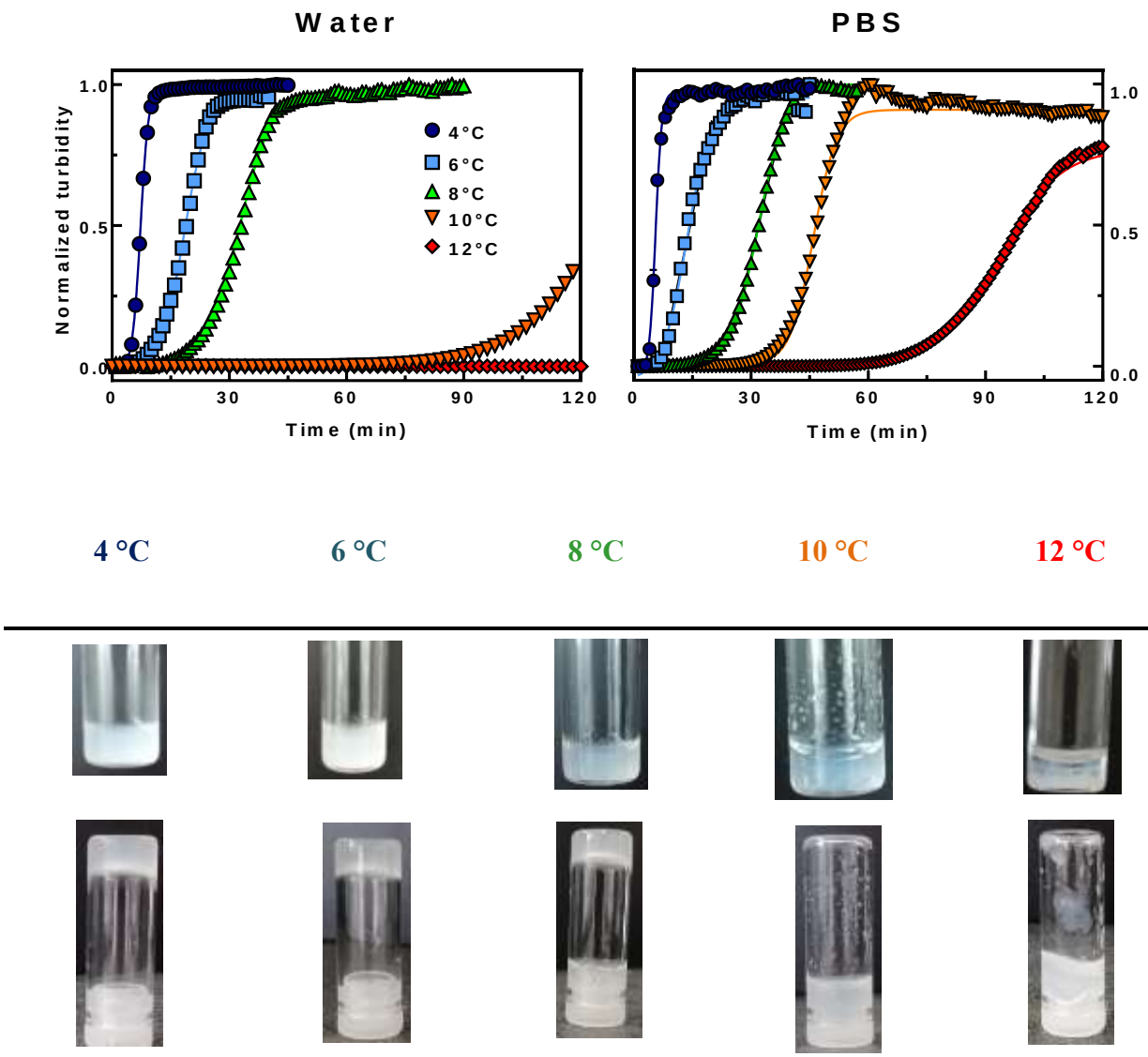

Figure 8. Gelation kinetics of BC at different temperature. Turbidity kinetics (top panel) at several temperatures in water (left) or PBS (right) and their visual aspects after 2 hours at each temperature (bottom panel) in PBS. Condition: [BC] = 1% w/v

In water (**Figure 8 top left**), BC can form a gel, with a slower kinetic as the temperature is increasing, from 4 °C to 8 °C. Above 8 °C, no gel turbidity appears clearly in water, meaning

that it is the critical temperature of gelation. At 10 °C, a slight increase in absorbance appears after 100 min and no turbidity is measurable at 12 °C after two hours. In PBS (**Figure 8 top right**), the kinetic of turbidity is quite in good agreement with the rheometry-based kinetic at 4 °C (**Figure 6 top & Figure S18)**. The turbidity is concomitant with the start of the gelation process, even though there are some delays between maximum turbidity and complete gelation. The increasing turbidity occurs even at 12 °C but does not reach the same plateau amplitude of turbidity as colder temperature. At 10 °C and above, the visual aspect of BC sample does not correspond to a gel, but more like floating aggregates and amorphous precipitates in an inhomogeneous suspension (**Figure 8 bottom**). These suspensions are also formed when BC solution is left at room temperature for at least 12h. To assess the impact of salt and pH on kinetic, BC 1% w/v in phosphate buffer at 10 mM and NaCl 0.9% w/v kinetic were performed and show ionic strength accelerate gelation (**Figure S1**).

The gel formation with these gelators is time-temperature dependent, where a ΔT is required as a thermodynamic force to start nucleation, but this temperature gradient needs to be restricted in an amount of time to ensure a propagative and homogenous fibrilogenesis in the whole volume (**Figure 8 bottom**). Unless, the self-assembling process will progressively form isolated aggregates of entangled fibers. Consequently, the T_c for BC is chosen as the minimal temperature where 1) $\Delta T = T_m - T_c$ is the smallest; 2) the gel is formed relatively fast (< 30 min) and homogeneously. From these requirements, the T_c reported for BC is 6 °C.

These results show the temperature dependency of gelation for different kinds of GNB but also some kinetic parameters that are linked to gelation rate. In general, a crystal formation process is driven by a thermodynamic force called supersaturation, when a change in solubility occurs at a temperature below the solubility limit temperature. In the same way, for gelators, at a given set

temperature T_{set} below the T_m, the gelation occurs because of a thermodynamic force defined by $\Delta T = T_m - T_{set}$, called supercooling[52]. The smallest amplitude of temperature needed for complete gelation corresponds to a hysteresis ΔT where T_{set} is at least equal to T_c. Nonetheless, supercooling amplitude is a crucial parameter for nucleation and fibrilogenesis rate. Also, it has to occur within a certain range of time to lead to a homogeneous metastable gel state. As a result, the fast gelation of BA 1% w/v (3 min) and BU 1% w/v (40 s) gelators at room temperature after melting at 82 °C, previously determined[28] and mentioned as gelation kinetic, may in fact refer to the time that is needed for the melted solution to cool down from T_m to T_{set} (T_{set} usually being the room temperature). It takes approximately 40 s for BU 1% w/v to cool down from 80 °C to 60 °C and 5 min for the BA 1% w/v to cool down from 80 °C to 40 °C, when they are held at room temperature. In a constant ramp of temperature of 1 °C min^{-1} as used for turbidimetry, cooling from T_m to the T_c takes 20 min during which gelators remain in sol phase. Therefore, gelation kinetic greatly depends on the timescale of the transition temperature gradient.

1.3.Calorimetry

Table 1. DSC data**.** The temperatures correspond to the maximum and minimum of the peaks and valleys of heat flow. Temperature ramp: 1 °C min^{-1}. NF = Not Found. As explained in the text, BC do not exhibit peak during cooling ramp.

		Water				**PBS**			
		T_m (°C)	**T_c (°C)**	**ΔH_m (mJ)**	**ΔH_c (mJ)**	**T_m (°C)**	**T_c (°C)**	**ΔH_m (mJ)**	**ΔH_c (mJ)**
BU	**1% w/v**	77.5 (±0.4)	58.8 (±0.8)	-13.3 (±3.8)	19.5 (±0.8)	82.0 (±0.1)	62.5 (±0.5)	-13.1 (±5.0)	16.3 (±4.2)
	2% w/v	78.5 (±0.5)	65.8 (±1.0)	-60.6 (±14.3)	75.5 (±19.5)	82.8 (±0.4)	62.7 (±0.3)	-44.1 (±6.6)	59.6 (±5.2)
BA	**1% w/v**	60.2 (±0.3)	36.9 (±2.4)	-15.9 (±1.8)	13.3 (±4.6)	61.8 (±0.4)	40.5 (±0.5)	-20.6 (±3.2)	14.07 (±0.7)
	2% w/v	61.0 (±0.1)	41.6 (±5.9)	-46.4 (±0.6)	44.1 (±2.4)	62.0 (±0.1)	42.5 (±2.1)	-40.9 (±0.9)	38.8 (±2.2)
BC	**1% w/v**	18.5 (±0.2)	NF	-9.8 (±1.2)	NF	25.6 (±0.9)	NF	-17.3 (±3.1)	NF
	2% w/v	18.4 (±0.1)	NF	-13.7 (±2.8)	NF	25.5 (±0.5)	NF	-41.3 (±3.3)	NF

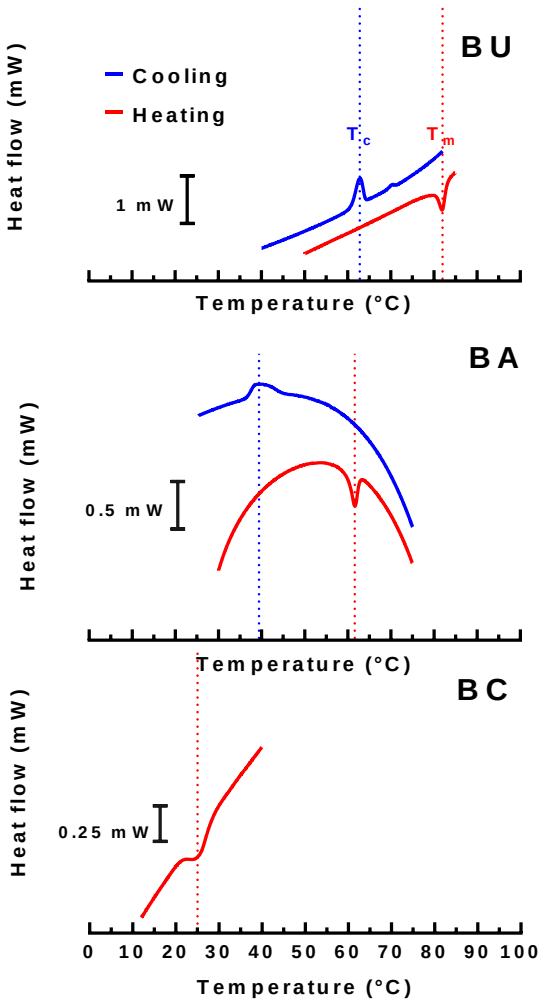

Figure 9. Differential scanning calorimetry experiments. Calorigrams of BU (top panel), BA (middle panel), BC (bottom panel) in PBS. Heating (red) and cooling (blue) cycles are arbitrary separated for clarity reasons. Condition: [GNB] = 2% w/v. Temperature ramp = 1 °C min^{-1}.

Heat exchange measurements constitute an important characterization of the temperature-phase relationship. DSC experiments were conducted in order to relate the data obtained from turbidimetry, which focus on visual aspects of the gels, to heat exchange processes. **Table 1** shows temperatures of phase transition T_m et T_c for each gelator, with these clear thermal

hysteresis. These data are in agreement with the optical transition measured by turbidimetry at 1% and 2% w/v, meaning that the visual change in turbidity actually relates to a thermodynamic mechanism. The thermal hysteresis is almost constant for all these gelators, with a $\Delta T \approx 20$ °C. For the same reason as mentioned above (slow process), the BC could not show any exothermic process during the cooling ramp and needed an isothermal ramp at 4 °C to show a positive peak of heat flow (**Figure S2**). For the BA, the T_m and T_c remain constant whether it is in water or PBS, whereas for BU and BC the T_m is shifted, from 78 °C in water to 82 °C in PBS for BU and from 18 °C in water to 25 °C in PBS for the BC 1% w/v. Noteworthy that BC in water shows two heat peak during melting, one at 18 °C and a slight second at 25 °C (**Figure S3**). Its melting could involve two distinct mechanisms that release heat: a first corresponding to the loss of interfibrillar interactions, and a second corresponding to intermolecular disassembling. Although, only the first peaks were reported in Table 1 since it corresponds to the first temperature where heat is exchanged and because of a sharper peak than the second. By integrating the heat flow peaks, ΔH_m and ΔH_c are determined as the heat energy released or consumed during melting and self-assembling respectively. Comparing 1% to 2% w/v concentrations, ΔH_m and ΔH_c do not seem to follow a trend and they are not significantly different between water and PBS (**Table 2**). Interestingly, the ΔH_m and ΔH_c also do not seem to significantly differ between these gelators when checked in the same condition of concentration and solvent. Differences in thermal stability depend on the linker, but same amount of energy involved in gelation and solubilization could mean that the energies of melting and self-assembling measured here are likely to correspond respectively to the energies of fibers organization and fibers disassembly, rather than molecular interactions energy. Also, there are dependencies on the temperature ramp, shown by the fact that a ramp of 0.5 °C min^{-1} seems too slow to show detectable heat exchange process

(data not shown) but a ramp of 2 °C min^{-1} or 5 °C min^{-1} accentuates the curves of heat flow and shift the transition temperatures compared to the ramp of 1 °C min^{-1} (**Figure S4**). This was observed in other cases with organogelators[53], and can be explained by the thermal inertia of the crucibles, but also by the fact that the state transition is indeed time-dependent and impacted by the temperature gradient. To probe the thermal inertia of crucibles, we measured heating cycle of azobenzene at these temperature ramps (**Figure S5**). It shows that the thermal inertia seems too low to be the main explanation of these shifts in transition temperature. A high cooling rate will shift the T_c in lower values and increase the supercooling because the gelator will require more time to self-assemble, complete nucleation then growth to form the gel. In contrast, a low cooling rate will give enough time to the gelator to nucleate and self-assemble, although it has to be sufficiently high in order to propagate in the whole volume and not shrink.

2. Circular dichroism

    2.1.Conformational analysis

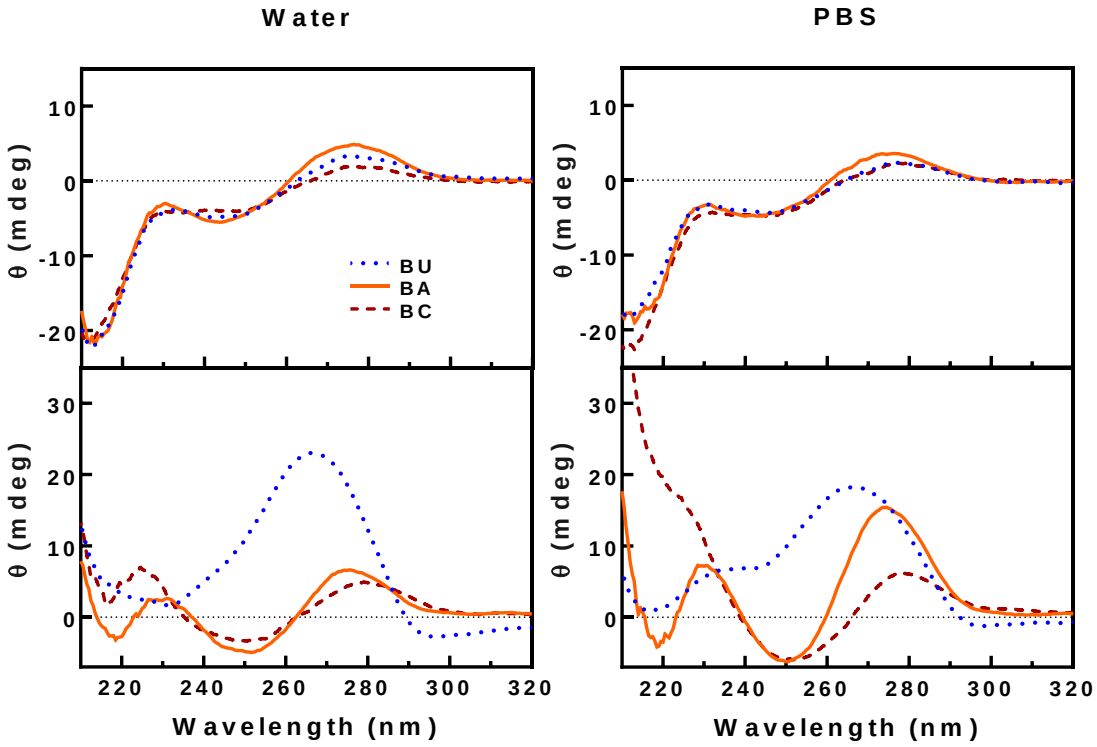

Figure 10. CD spectra of BU (blue dotted line), BA (orange solid line) and BC (red dashed line) at 0.05% w/v in water (left panels) or in PBS (right panels) solubilized (top panels) or self-assembled (bottom panels).

The nature of the linker in the GNB structure plays an important role on the structural assembly. CD can contribute to the characterization of the structuration of LMWG at supramolecular level. In both pure water or PBS, CD spectra acquired at 80 °C to ensure complete solubilization show the same ellipticity, with valleys at 212 and 243 nm, and bands at 230 and 276 nm (**Figure 10 top**). High tension voltage (HT) data are reported in ESI (**Figure S19**). These signals were previously assigned as corresponding to specific ellipticity bands of thymidine and its derivatives[24]. In the longest wavelength (> 250 nm), the CD signal of the thymidine base was associated with an oriented $\pi \rightarrow \pi^*$ transition within the aromatic ring[54,55]. These show that the glyco-nucleoside chromophore they have in common contributes to their CD

spectra. Consequently, they exhibit the same ellipticity when they are solubilized in both water or PBS, their common moiety is freely exposed and excited in the same way.

When assembled, each gelator shows its own different supramolecular chirality according to its ellipticity signal (**Figure 10 bottom**). The BU has a positive band shifted to 265 nm in both pure water and PBS, but the valley at 230 nm in water is inverted into a shoulder and shifted to 232 nm in PBS. The BA and BC share similar ellipticity signature in water, with some subtle differences regarding the wavelength of their peaks: bands at 275 and 230 nm, and valleys at 251 and 218 nm for the BA; bands at 279 and 225 nm, and valleys at 250 and 217 nm for the BC. Moreover, BC exhibits a complete peak inversion at 212 nm and higher intensity in PBS. When solubilized, these gelators have an absorption peak at λ_{max} = 267 nm, corresponding to the modified thymine nucleobase present twice in those molecules, with an attenuation coefficient quite similar to two thymidine nucleosides ($\varepsilon \approx 18\,000$ L cm^{-1} mol^{-1}). During the self-assembling, the λ_{max} is slightly shifted as a hypsochromic effect, with a $\Delta\lambda \approx 5$nm (**Figure S6**). These results show that with the same global « backbone structure », the nature of the linker that differs between those gelators influences the conformational features. The linkers might impact as well the relative orientation of the whole glyco-nucleoside moiety along the axis of the fibers during self-interaction. The changes in direction of $\pi \rightarrow \pi^*$ transitions are shown by the different shifts in wavelength of the ellipticity peaks between these three gelators. The nature of the linking moiety impacts the promotion of base stacking or hydrogen-bonding, leading to differences in chirality and physical properties. More interactions at molecular level give more mechanical and thermal stability to the assembly. The differences between supramolecular chirality in water or PBS show that conformation might also be affected by the nature of the solvent. Since the fibrilogenesis involves molecule-molecule interactions but also molecule-solvent interactions[31], adding a pH

buffer and/or ionic strength might change the way water molecule solvation occurs or the protons exchanges that are involved in hydrogen-bonding. In that way, if the solvent impacts the hydrogelator features at any scale, it is important to evaluate their influence on the gel properties. For instance, in a purpose of biological application, knowing the impact of the buffer is crucial.

2.2.Thermal stability at the supramolecular level

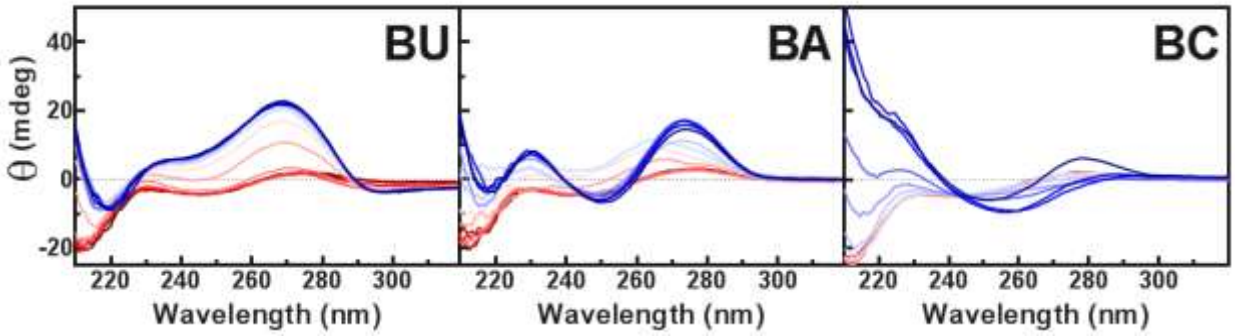

Figure 11. Melting CD scan of GNB. CD spectra of BU (left), BA (middle), BC (right) from cold (blue) to hot (red) temperatures. Condition: [GNB] = 0.05% w/v in PBS.

To investigate thermal stability at the supramolecular scale, CD scans with temperature ramps were done (**Figure 11; Figure S7-S8**). During the heating cycle, gelators are losing progressively their supramolecular chirality until they exhibit their solubilized spectrum after complete melting. In the cooling cycle, they remain soluble until a brutal change in chirality corresponding to their self-assembly. Then by plotting their ellipticity at a specific wavelength as a function of the temperature, we can access their thermodynamics parameters (**Figure 12**). Thermodynamics data are obtained by processing a Van't Hoff analysis on the thermal denaturation plots. The constant K at each temperature is expressed as

$$K = \frac{CD_\theta - CD_{sol}}{CD_f - CD_{sol}}$$

where CD_{sol} and CD_f corresponds respectively to the CD of solubilized and self-assembled GNB, and CD_θ is the CD monitored at each temperature. Van't Hoff plots are shown in **Figure S9** and the data are summed up in **Table 2**. The thermal hysteresis is still present for BU and BA and their self-assembling is also occurring in a non-isothermal process. At the supramolecular level, the thermal hysteresis can be attributed to the thermodynamic force that drives the first nucleations. The melting and self-assembling points of BU and BA are very different from these of the other acquisitions from previous techniques. T_m is dropped from 80 °C and 60 °C to 50 °C and 30 °C, and T_c is dropped from 60 °C and 40 °C to 35 °C and 20 °C, for BU and BA respectively. The greater melting enthalpy of BU is consistent with its ability to form additional hydrogen bonds. The more negative value of entropy for BU and BA in PBS compared to water can be attributed to a more ordered structure due to solvation effects.

The BC melts at around 20 °C but as expected no supramolecular chirality recovery was observed during cooling cycle. Although, at 4 °C its self-assembling occurs in PBS and in water, although slower in water (**Figure 13**). The nature of the solvent seems to impact thermal stability, with different transition temperatures between water and PBS conditions, but also the kinetic of self-assembling.

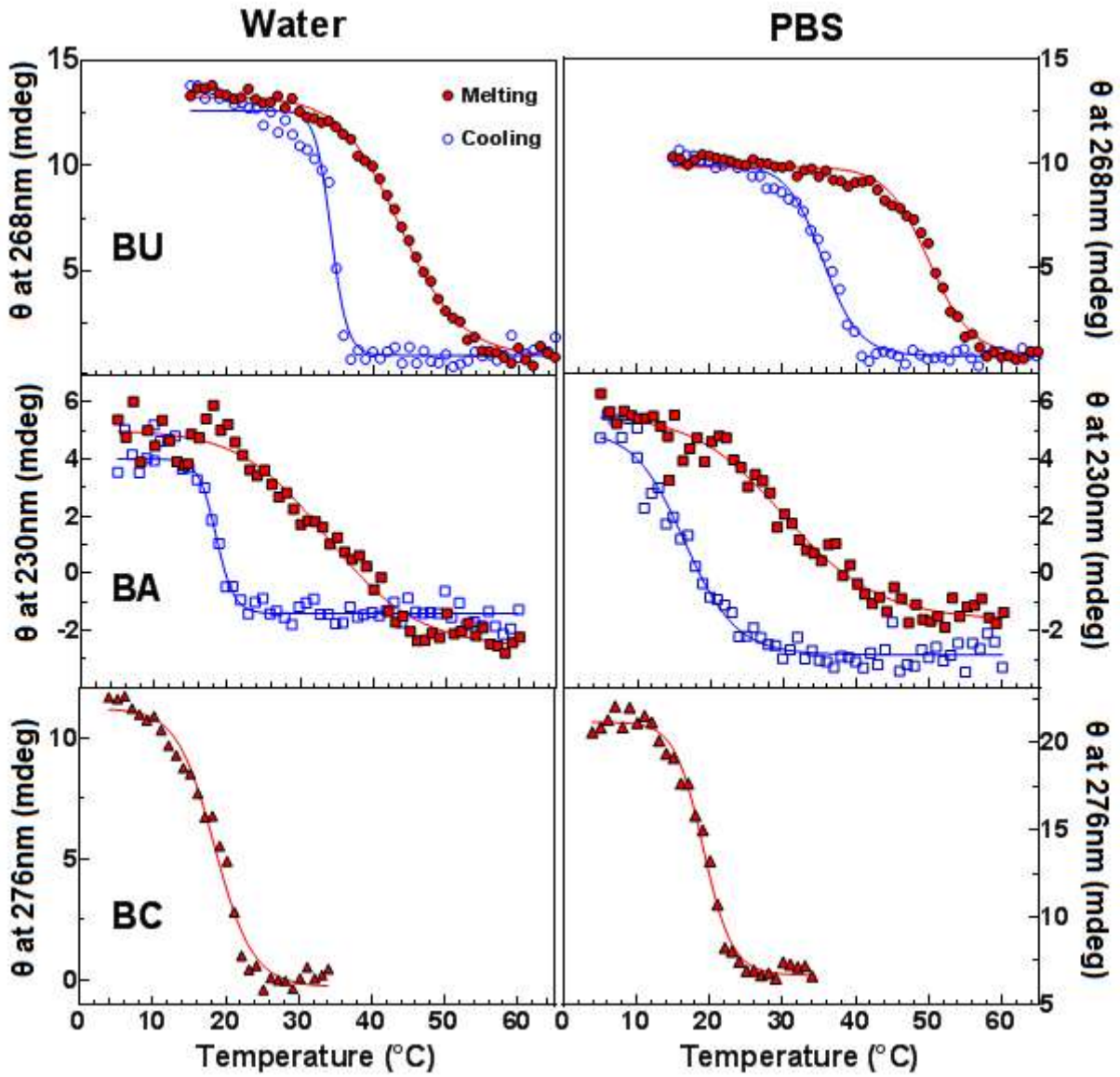

Figure 12. CD thermal denaturation of GNB. CD signal function of temperature with BU (top panels), BA (middle panels) and BC (bottom panels), heating (red) or cooling (blue) in water (left panels) or PBS (right panels). Condition: [GNB] = 0.05% w/v

	Water				PBS			
	T_m (°C)	T_c (°C)	ΔH (kcal mol^{-1})	ΔS (cal K^{-1} mol^{-1})	T_m (°C)	T_c (°C)	ΔH (kcal mol^{-1})	ΔS (cal K^{-1} mol^{-1})
BU	43.7	34.2	-24.4	-78.5	50.1	35.5	-32.2	-122.8
BA	33.9	18.4	-16.3	-31.3	30.4	16.5	-14.1	-48.1
BC	18.5	-	-13.1	-46.3	19.1	-	-12.5	-43.1

Table 2. Thermodynamics parameters of GNB at 0.05% w/v. Data from Van't Hoff analysis of CD thermal denaturation.

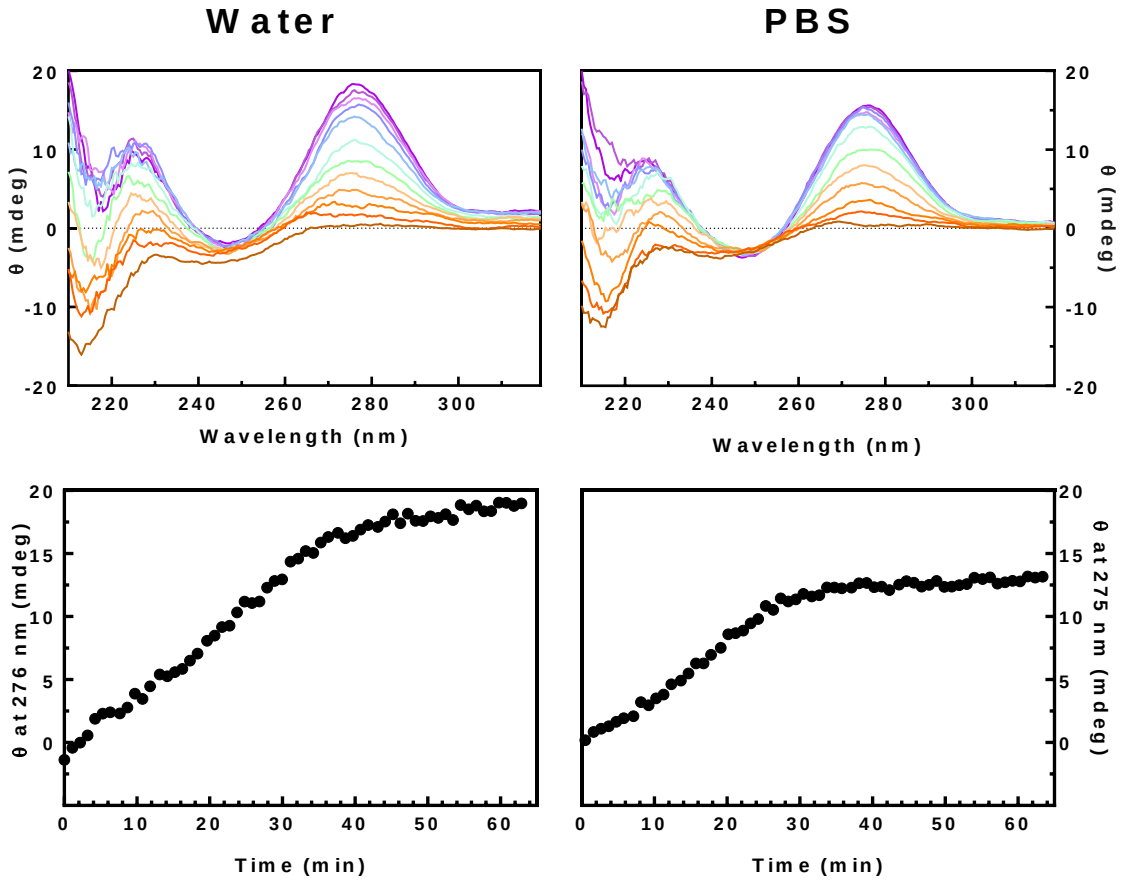

Figure 13. CD kinetics of BC at 4 °C. CD scan interval (top panels) of BC in water (left) or PBS (right) every 5 min during 1h (from dark orange to purple) and their plots at specific wavelength

function of time (bottom panels). Condition: [BC] = 0.05% w/v. Time interval: 5 min between each scan and 1 min between each data points of plot.

The UV absorption spectra obtained with these temperatures ramp show a hypsochromic effect as mentioned above, for all the gelators, at low temperature, when they self-assemble. BU exhibits a hyperchromic effect during heating and hypochromic effect during cooling (**Figure S6**). The nucleobase of the BU gelator might be involved in base π-stacking, that might explain higher thermal stability of this gelators compared to the two others, in addition to the urea moieties adding hydrogen-bond sites. The blue shift in λ_{max} noticed for all the GNB translates a change in energy of $\pi \rightarrow \pi^*$ electronic transition of the thymidine moiety because of its involvement in intermolecular interactions.

3. Discussion

The transition temperatures determined by different techniques are quite different from one to another for two main reasons: 1) thermal stability depends on the concentration, therefore the difference can be explained by the different concentration used in those techniques (1% w/v and 2% w/v in calorimetry *vs* 0.05% w/v in CD); 2) each technique does not measure and monitor the same feature. Rheometry measures viscoelastic moduli that are related to the macroscopic and mesoscopic organization of the mesh formed by fibers entanglement. Moreover, stress and strain conditions under the cone-plate geometry might also influence the gelation process during thermal cycles, explaining the shift in phase transition temperature compared to DSC for

instance. During a controlled stress experiment, the strain amplitude will adapt to the measurement in order to keep a decent signal to noise ratio. As the sample is weakened by the temperature, the strain amplitude will increase, but doing so will also contribute to the weakening of the sample. That explains why BA for example have smaller values of $T_{gel\text{-}sol}$ in controlled stress than in controlled strain amplitude, the latter being fixed at the lowest, but also why it does not cure at every frequency during cooling in controlled stress condition, knowing that the strain amplitude is still high enough during cooling, hindering the gelation. The signal is cleaner in controlled stress because of the increase of strain amplitude upon transition, but is still too variable. Since other techniques do not apply any mechanical stress and the sample is not undergoing any strain, differences between rheology and other techniques are expected, even though the constant strain amplitude experiment can give closer results to other experiments, that is actually quite the case. CD probes changing features at the molecular scale, so the transitions are more likely to correspond to changes in supramolecular chirality induced by self-assembling or disassembling. Thus, it is a quite interesting technique to probe the first moments of nucleation right before the growth stage, since it is sensitive enough to change its signal as soon as supramolecular interactions occur. Although the conditions of experiments (*i.e.* concentration, solvent) are limited by the CD spectrophotometer and the absorbance of the sample; hence it can require some specific equipment to manipulate in more gel-like conditions (i.e. low optical length, synchrotron radiation…).

By turbidimetry, temperature ramps were done on a wide range of concentrations to evaluate the influence of the concentration on phase transition temperature (**Figure S10-S12**). T_m and T_c at 0.05% w/v are in agreement with the CD experiments. Phase diagrams are represented by pooling the different phase transition temperatures determined by all those techniques

(**Figure 14**) and show the dependency of the concentration on the phase-transition temperatures. Sol phase is represented by the part of the diagram above the T_m determined at each concentration. In the same way, the self-assembled gelators phase (fibers or gel above critical gelation concentration) corresponds to the part of the diagram below the T_c. The phase in white part of the diagram depends on which temperature cycle (heating or cooling) the gelators are following and which is the phase at the beginning of the cycle.

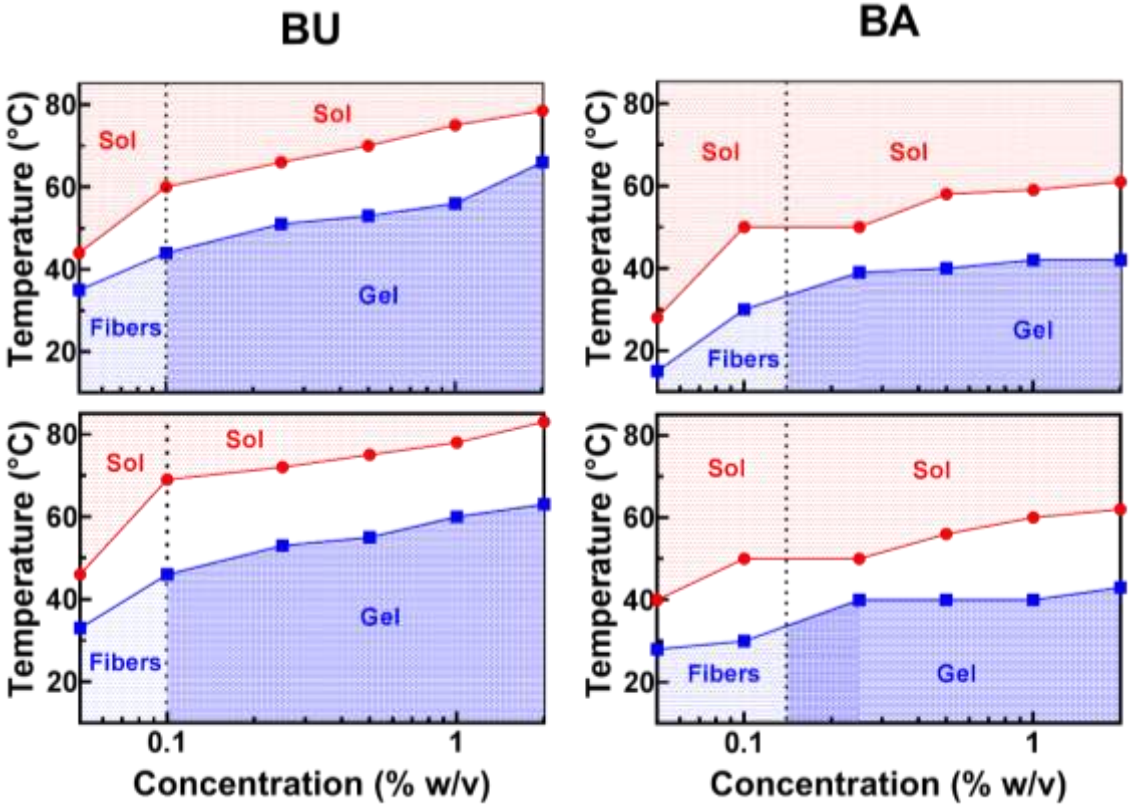

Figure 14. Phase diagrams. T_m and the T_c function of concentration of BU (left panels) or BA (right panels) in water (top panels) or in PBS (bottom panels). Vertical dashed plot corresponds to the critical gelation concentration (CGC). Red line separating the sol phase part and blue line separating the self-assembled part correspond to the T_m and the T_c, respectively. The white part of the diagrams represents the hysteresis.

The temperatures of phase transition are lower as the concentration decrease. This observation highlights the fact that phase transition temperatures are influenced by the intermolecular stability but also by the interfibrillar interactions. By diminishing the quantity of fibers, the amount of energy required to solubilize the network will decrease. It is consistent with the thermal stability assessed by CD in diluted conditions, where the acquired transition temperatures are lower than in other techniques and correspond to intermolecular stability of the self-assembled units. Moreover, it seems like there are two different regime of transition temperature evolution, above and below the CGC, but lack of data in more diluted conditions makes it difficult to conclude this way. In more practical considerations, knowing the concentration dependencies of transition temperatures can clarify the range of applications of these hydrogels, *e.g.* using gels in low concentrations means that the melting temperature is lowered, but also the supercooling can take more times to permit the gelation at room temperature, so they can be easily manipulated in a wider range of time.

Finally, and interestingly, the turbidity curves in lower concentrations often show two inflexions during melting (**Figure S10-S12**). This can be explained by a two-step transition upon heating cycle, first transition could correspond to interfibrillar interactions weakening, leading to a drop in turbidity, and second transition corresponds to intermolecular disassembling and complete solubilization. The following table (**Table 3**) summarize the properties of GNB studied.

Table 3. Summary of GNB properties

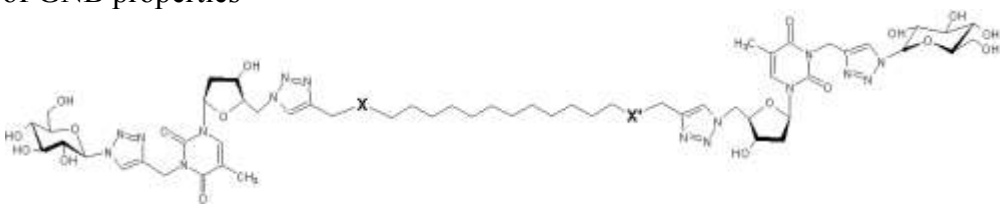

X, X'	Urea	Amide	Carbamate
Abbreviation	**BU**	**BA**	**BC**
Relative stiffness G' (kPa) at 1% w/v	Stiffest (52.4 ±12.7, at 25 °C)	Moderate (4.0 ±2.0, at 25 °C)	Softest (1.0 ±0.6, at 10 °C)
T_m / T_c at 1% w/v	80 °C / 60 °C	60 °C / 40 °C	25 °C / 6 °C
T_m / T_c at 0.25% w/v	65 °C / 55 °C	50 °C / 40 °C	20 °C
Time-temperature dependency	Non-isothermal, fast gelation upon cooling (supercooling)	Non-isothermal, fast gelation upon cooling (supercooling)	Isothermal gelation, faster gelation at lower temperature
Effect of saline solution on gelation	Slightly higher thermal stability, higher fibers ordering, change in supramolecular assembling	Higher fibers ordering, change in supramolecular assembling	Change in supramolecular assembling, acceleration of the gelation kinetic
Microscopic features	Spectral signature of base-stacking interaction, high fibers branching	Fiber joints	1-dimensional growth with potential fibers branching based on Avrami model

Conclusion

The GNB hydrogelators that were studied, differ only by the small moiety that links the hydrophobic and the hydrophilic segments they have in common. These differences impacting mechanical properties, but also thermal and kinetic stability, were assessed by different techniques. All these hydrogelators display different phase transition temperatures and a thermal hysteresis, phase transition depending greatly on the path followed. For the urea and amide based GNB (BU and BA), the gelation process is kinetically fast and non-isothermal since the thermodynamic forces mainly contribute to it. Thermodynamic force and thermal hysteresis seem to be related to the supercooling process, similar to supersaturation in the case of crystallization, that consists of time dependent temperature gradient that drives nucleation and fibrilogenesis of these GNB. For the carbamate based GNB (BC), the gelation occurs at low temperature in an isothermal process and thus exhibits a measurable kinetic. Noteworthy that the time dependency is translated by the fact that temperature cycles with a low ramp, tend to form scatter aggregates, instead of a homogeneous gel brought by a sufficiently fast temperature gradient. In addition to the thermal properties assessment, conformational study was conducted by circular dichroism spectroscopy in order to relate the molecular structure of the GNB to their supramolecular assembly. It showed that the different GNB lead to different supramolecular chirality. The differences in self-structuring result from a possibility of intermolecular interactions which differ according to the nature of the linker. By promoting or not certain interactions, this leads to different stabilities, that were also assessed by temperature scan of CD signal. Finally, alongside the nature of the molecule, the solvent conditions and the concentration play a major role in the thermal and kinetic properties of these GNB. This study gives another

view on the hydrogelation characteristics of these GNB, especially about the thermodynamic and kinetic properties, that can be of interest to determine the range of applications, but also some interesting conformational information brought by CD. Though, those properties need to be rationalized to fully understand the mechanisms at work in gelation process, further studies will be needed. Nonetheless, this study gives another argument in favor of more exhaustive list of information about the gelation protocols that are reported, such as cooling rate and temperature of isothermal gelation, controlled parameters of rheology based experiments, as well as the type of container. Indeed, many of these parameters have an impact on the gelation, for example different mechanical stress can influence the network formation in a way that could skew the measurement, and containers with different volume distribution and surface materials can impact the heat dynamics, hence affect gelation, especially of thermally driven gels. These are expected to be kept in mind and mentioned, for the sake of reproducibility.

Supporting Information

Gelation kinetics, calorigrams, UV and CD spectra, Van't Hoff plots, turbidimetry and rheology.

Author Information

Corresponding authors:

* E-mail: bruno.alies@u-bordeaux.fr (B.A.); gaetane.lespes@univ-pau.fr (G.L.). Phone : (+33) 5 57 57 46 86 (B.A.); (+33) 5 59 40 76 71 (G.L.).

Acknowledgment

This work has been supported by “Region Nouvelle-Aquitaine” and “Ligue contre le Cancer Comité de Gironde”. Cryo-electronic Microscopy were done in the Bordeaux Imaging Center a service unit of the CNRS-INSERM and Bordeaux University, member of the national infrastructure France BioImaging supported by the French National Research Agency (ANR-10-INBS-04). We thank Julien Verget for synthesis of GNB molecules, Eve Descomps for data collection, Alexandra Gaubert for help with rheology and Isabelle Svahn for SEM microscopy.

References:

(1) Smith, D. K. Self-Assembling Fibrillar Networks—Supramolecular Gels. In *Supramolecular Chemistry*; American Cancer Society, 2012. https://doi.org/10.1002/9780470661345.smc142.

(2) Loos, M. de; Feringa, B. L.; Esch, J. H. van. Design and Application of Self-Assembled Low Molecular Weight Hydrogels. *Eur. J. Org. Chem.* **2005**, *2005* (17), 3615–3631. https://doi.org/10.1002/ejoc.200400723.

(3) Steed, J. W. Supramolecular Gel Chemistry: Developments over the Last Decade. *Chem. Commun.* **2011**, *47* (5), 1379–1383. https://doi.org/10.1039/C0CC03293J.

(4) Maisani, M.; Ziane, S.; Ehret, C.; Levesque, L.; Siadous, R.; Le Meins, J.-F.; Chevallier, P.; Barthélémy, P.; De Oliveira, H.; Amédée, J.; Mantovani, D.; Chassande, O. A New Composite Hydrogel Combining the Biological Properties of Collagen with the Mechanical Properties of a Supramolecular Scaffold for Bone Tissue Engineering. *J. Tissue Eng. Regen. Med.* **2018**, *12* (3), e1489–e1500. https://doi.org/10.1002/term.2569.

(5) Ziane, S.; Schlaubitz, S.; Miraux, S.; Patwa, A.; Lalande, C.; Bilem, I.; Lepreux, S.; Rousseau, B.; Le Meins, J.-F.; Latxague, L.; Barthélémy; Chassande, O. A Thermosensitive Low Molecular Weight Hydrogel as Scaffold for Tissue Engineering. *Eur. Cell. Mater.* **2012**, *23*, 147–160. https://doi.org/10.22203/eCM.v023a11.

(6) Zuidema, J. M.; Rivet, C. J.; Gilbert, R. J.; Morrison, F. A. A Protocol for Rheological Characterization of Hydrogels for Tissue Engineering Strategies. *J. Biomed. Mater. Res. B Appl. Biomater.* **2014**, *102* (5), 1063–1073. https://doi.org/10.1002/jbm.b.33088.

(7) Tibbitt, M. W.; Anseth, K. S. Hydrogels as Extracellular Matrix Mimics for 3D Cell Culture. *Biotechnol. Bioeng.* **2009**, *103* (4), 655–663. https://doi.org/10.1002/bit.22361.

(8) Ruedinger, F.; Lavrentieva, A.; Blume, C.; Pepelanova, I.; Scheper, T. Hydrogels for 3D Mammalian Cell Culture: A Starting Guide for Laboratory Practice. *Appl. Microbiol. Biotechnol.* **2015**, *99* (2), 623–636. https://doi.org/10.1007/s00253-014-6253-y.

(9) Geckil, H.; Xu, F.; Zhang, X.; Moon, S.; Demirci, U. Engineering Hydrogels as Extracellular Matrix Mimics. *Nanomed.* **2010**, *5* (3), 469–484. https://doi.org/10.2217/nnm.10.12.
(10) Latxague, L.; Ramin, M. A.; Appavoo, A.; Berto, P.; Maisani, M.; Ehret, C.; Chassande, O.; Barthélémy, P. Control of Stem-Cell Behavior by Fine Tuning the Supramolecular Assemblies of Low-Molecular-Weight Gelators. *Angew. Chem. Int. Ed.* **2015**, *54* (15), 4517–4521. https://doi.org/10.1002/anie.201409134.
(11) Kretlow, J. D.; Klouda, L.; Mikos, A. G. Injectable Matrices and Scaffolds for Drug Delivery in Tissue Engineering. *Adv. Drug Deliv. Rev.* **2007**, *59* (4), 263–273. https://doi.org/10.1016/j.addr.2007.03.013.
(12) Li, J.; Mooney, D. J. Designing Hydrogels for Controlled Drug Delivery. *Nat. Rev. Mater.* **2016**, *1* (12). https://doi.org/10.1038/natrevmats.2016.71.
(13) Nowak, A. P.; Breedveld, V.; Pakstis, L.; Ozbas, B.; Pine, D. J.; Pochan, D.; Deming, T. J. Rapidly Recovering Hydrogel Scaffolds from Self-Assembling Diblock Copolypeptide Amphiphiles. *Nature* **2002**, *417* (6887), 424. https://doi.org/10.1038/417424a.
(14) Ryadnov, M. G. Peptide Alpha-Helices for Synthetic Nanostructures. *Biochem. Soc. Trans.* **2007**, *35* (Pt 3), 487–491. https://doi.org/10.1042/BST0350487.
(15) Zhao, X.; Zhang, S. Designer Self-Assembling Peptide Materials. *Macromol. Biosci.* **2007**, *7* (1), 13–22. https://doi.org/10.1002/mabi.200600230.
(16) Gao, J.; Tang, C.; Elsawy, M. A.; Smith, A. M.; Miller, A. F.; Saiani, A. Controlling Self-Assembling Peptide Hydrogel Properties through Network Topology. *Biomacromolecules* **2017**, *18* (3), 826–834. https://doi.org/10.1021/acs.biomac.6b01693.
(17) Parisi, E.; Garcia, A. M.; Marson, D.; Posocco, P.; Marchesan, S. Supramolecular Tripeptide Hydrogel Assembly with 5-Fluorouracil. *Gels* **2019**, *5* (1), 5. https://doi.org/10.3390/gels5010005.
(18) Araki, K.; Yoshikawa, I. Nucleobase-Containing Gelators. *Top. Curr. Chem.* **2005**, *256*, 133–165. https://doi.org/10.1007/b107173.
(19) Campins, N.; Dieudonné, P.; W. Grinstaff, M.; Barthélémy, P. Nanostructured Assemblies from Nucleotide -Based Amphiphiles. *New J. Chem.* **2007**, *31* (11), 1928–1934. https://doi.org/10.1039/B704884J.
(20) Peters, G. M.; Davis, J. T. Supramolecular Gels Made from Nucleobase, Nucleoside and Nucleotide Analogs. *Chem. Soc. Rev.* **2016**, *45* (11), 3188–3206. https://doi.org/10.1039/C6CS00183A.
(21) Fages, F.; Vögtle, F.; Zinic, M. Systematic Design of Amide- and Urea-Type Gelators with Tailored Properties. *Top. Curr. Chem.* **2005**, *256*, 77–131. https://doi.org/10.1007/b107172.
(22) Godeau, G.; Brun, C.; Arnion, H.; Staedel, C.; Barthélémy, P. Glycosyl-Nucleoside Fluorinated Amphiphiles as Components of Nanostructured Hydrogels. *Tetrahedron Lett.* **2010**, *51* (7), 1012–1015. https://doi.org/10.1016/j.tetlet.2009.12.042.
(23) Latxague, L.; Dalila, M.-J.; Patwa, A.; Ziane, S.; Chassande, O.; Godeau, G.; Barthélémy, P. Glycoside Nucleoside Lipids (GNLs): An Intrusion into the Glycolipids' World? *Comptes Rendus Chim.* **2012**, *15* (1), 29–36. https://doi.org/10.1016/j.crci.2011.08.010.
(24) Alies, B.; Ouelhazi, M. A.; Patwa, A.; Verget, J.; Navailles, L.; Desvergnes, V.; Barthélémy, P. Cytidine- and Guanosine-Based Nucleotide–Lipids. *Org. Biomol. Chem.* **2018**, *16* (26), 4888–4894. https://doi.org/10.1039/C8OB01023D.

(25) Baillet, J.; Desvergnes, V.; Hamoud, A.; Latxague, L.; Barthélémy, P. Lipid and Nucleic Acid Chemistries: Combining the Best of Both Worlds to Construct Advanced Biomaterials. *Adv. Mater.* **2018**, *30* (11), 1705078. https://doi.org/10.1002/adma.201705078.

(26) Latxague, L.; Gaubert, A.; Maleville, D.; Baillet, J.; Ramin, M.; Barthélémy, P. Carbamate-Based Bolaamphiphile as Low-Molecular-Weight Hydrogelators. *Gels* **2016**, *2* (4), 25. https://doi.org/10.3390/gels2040025.

(27) Ochi, R.; Kurotani, K.; Ikeda, M.; Kiyonaka, S.; Hamachi, I. Supramolecular Hydrogels Based on Bola-Amphiphilic Glycolipids Showing Color Change in Response to Glycosidases. *Chem. Commun.* **2013**, *49* (21), 2115–2117. https://doi.org/10.1039/C2CC37908B.

(28) Ramin, M. A.; Latxague, L.; Sindhu, K. R.; Chassande, O.; Barthélémy, P. Low Molecular Weight Hydrogels Derived from Urea Based-Bolaamphiphiles as New Injectable Biomaterials. *Biomaterials* **2017**, *145*, 72–80. https://doi.org/10.1016/j.biomaterials.2017.08.034.

(29) Chalard, A.; Vaysse, L.; Joseph, P.; Malaquin, L.; Souleille, S.; Lonetti, B.; Sol, J.-C.; Loubinoux, I.; Fitremann, J. Simple Synthetic Molecular Hydrogels from Self-Assembling Alkylgalactonamides as Scaffold for 3D Neuronal Cell Growth. *ACS Appl. Mater. Interfaces* **2018**, *10* (20), 17004–17017. https://doi.org/10.1021/acsami.8b01365.

(30) Weiss, R. G. The Past, Present, and Future of Molecular Gels. What Is the Status of the Field, and Where Is It Going? *J. Am. Chem. Soc.* **2014**, *136* (21), 7519–7530. https://doi.org/10.1021/ja503363v.

(31) Zurcher, D. M.; McNeil, A. J. Tools for Identifying Gelator Scaffolds and Solvents. *J. Org. Chem.* **2015**, *80* (5), 2473–2478. https://doi.org/10.1021/jo502915w.

(32) Draper, E. R.; Adams, D. J. Controlling the Assembly and Properties of Low-Molecular-Weight Hydrogelators. *Langmuir* **2019**, *35* (20), 6506–6521. https://doi.org/10.1021/acs.langmuir.9b00716.

(33) Raeburn, J.; Cardoso, A. Z.; Adams, D. J. The Importance of the Self-Assembly Process to Control Mechanical Properties of Low Molecular Weight Hydrogels. *Chem. Soc. Rev.* **2013**, *42* (12), 5143–5156. https://doi.org/10.1039/C3CS60030K.

(34) Tang, C.; Smith, A. M.; Collins, R. F.; Ulijn, R. V.; Saiani, A. Fmoc-Diphenylalanine Self-Assembly Mechanism Induces Apparent PKa Shifts. *Langmuir ACS J. Surf. Colloids* **2009**, *25* (16), 9447–9453. https://doi.org/10.1021/la900653q.

(35) Weiss, R. G. Controlling Variables in Molecular Gel Science: How Can We Improve the State of the Art? *Gels* **2018**, *4* (2). https://doi.org/10.3390/gels4020025.

(36) Liyanage, W.; Brennessel, W. W.; Nilsson, B. L. Spontaneous Transition of Self-Assembled Hydrogel Fibrils into Crystalline Microtubes Enables a Rational Strategy To Stabilize the Hydrogel State. *Langmuir* **2015**, *31* (36), 9933–9942. https://doi.org/10.1021/acs.langmuir.5b01953.

(37) van Esch, J. H. We Can Design Molecular Gelators, but Do We Understand Them? *Langmuir ACS J. Surf. Colloids* **2009**, *25* (15), 8392–8394. https://doi.org/10.1021/la901720a.

(38) Hashemnejad, S. M.; Kundu, S. Probing Gelation and Rheological Behavior of a Self-Assembled Molecular Gel. *Langmuir* **2017**, *33* (31), 7769–7779. https://doi.org/10.1021/acs.langmuir.7b01531.

(39) Lommel, R. V.; Zhao, J.; Borggraeve, W. M. D.; Proft, F. D.; Alonso, M. Molecular Dynamics Based Descriptors for Predicting Supramolecular Gelation. *Chem. Sci.* **2020**, *11* (16), 4226–4238. https://doi.org/10.1039/D0SC00129E.
(40) NAGARAJAN, R. Self-Assembly of Bola Amphiphiles. *Chem. Eng. Commun.* **1987**, *55* (1–6), 251–273. https://doi.org/10.1080/00986448708911931.
(41) Winter, H. H.; Chambon, F. Analysis of Linear Viscoelasticity of a Crosslinking Polymer at the Gel Point. *J. Rheol.* **1986**, *30* (2), 367–382. https://doi.org/10.1122/1.549853.
(42) Winter, H.; Mours, M. Rheology of Polymers near Liquid-Solid Transitions. *NEUTRON SPIN ECHO Spectrosc. VISCOELASTICITY Rheol.* **1997**, *134*. https://doi.org/10.1007/3-540-68449-2_3.
(43) Yan, Z.-C.; Biswas, C. S.; Stadler, F. J. Rheological Study on the Thermoreversible Gelation of Stereo-Controlled Poly(N-Isopropylacrylamide) in an Imidazolium Ionic Liquid. *Polymers* **2019**, *11* (5). https://doi.org/10.3390/polym11050783.
(44) He, Y.; Lodge, T. P. A Thermoreversible Ion Gel by Triblock Copolymer Self-Assembly in an Ionic Liquid. *Chem. Commun.* **2007**, No. 26, 2732–2734. https://doi.org/10.1039/B704490A.
(45) Fuentes-Caparrós, A. M.; Gómez-Franco, F. de P.; Dietrich, B.; Wilson, C.; Brasnett, C.; Seddon, A.; Adams, D. J. Annealing Multicomponent Supramolecular Gels. *Nanoscale* **2019**, *11* (7), 3275–3280. https://doi.org/10.1039/C8NR09423C.
(46) Avrami, M. Kinetics of Phase Change. II Transformation- Time Relations for Random Distribution of Nuclei. *J. Chem. Phys.* **1940**, *8* (2), 212–224. https://doi.org/10.1063/1.1750631.
(47) Fanfoni, M.; Tomellini, M. The Johnson-Mehl- Avrami-Kohnogorov Model: A Brief Review. *Il Nuovo Cimento D* **1998**, *20* (7), 1171–1182. https://doi.org/10.1007/BF03185527.
(48) Hillier, I. H. Modified Avrami Equation for the Bulk Crystallization Kinetics of Spherulitic Polymers. *J. Polym. Sci. A* **1965**, *3* (9), 3067–3078. https://doi.org/10.1002/pol.1965.100030902.
(49) Yang, J.; McCoy, B. J.; Madras, G. Distribution Kinetics of Polymer Crystallization and the Avrami Equation. *J. Chem. Phys.* **2005**, *122* (6), 064901. https://doi.org/10.1063/1.1844373.
(50) Liu, Y.; Wang, R.-Y.; Li, J.-L.; Yuan, B.; Han, M.; Wang, P.; Liu, X.-Y. Identify Kinetic Features of Fibers Growing, Branching, and Bundling in Microstructure Engineering of Crystalline Fiber Network. *CrystEngComm* **2014**, *16* (24), 5402–5408. https://doi.org/10.1039/C4CE00096J.
(51) Okesola, B. O.; Wu, Y.; Derkus, B.; Gani, S.; Wu, D.; Knani, D.; Smith, D. K.; Adams, D. J.; Mata, A. Supramolecular Self-Assembly To Control Structural and Biological Properties of Multicomponent Hydrogels. *Chem. Mater.* **2019**, *31* (19), 7883–7897. https://doi.org/10.1021/acs.chemmater.9b01882.
(52) Rastogi, R. Thermodynamics of Metastable Equilibria (Metastability-Supersaturation, Nucleation and Crystallization)*. 6.
(53) De la Peña-Gil, A.; Álvarez-Mitre, F. M.; González-Chávez, M. M.; Charó-Alonso, M. A.; Toro-Vazquez, J. F. Combined Effect of Shearing and Cooling Rate on the Rheology of Organogels Developed by Selected Gelators. *Food Res. Int.* **2017**, *93*, 52–65. https://doi.org/10.1016/j.foodres.2017.01.010.

(54) Greve, J.; Maestre, M. F.; Levin, A. Circular Dichroism of Adenine and Thymine Containing Synthetic Polynucleotides. *Biopolymers* **1977**, *16* (7), 1489–1504. https://doi.org/10.1002/bip.1977.360160709.
(55) Sprecher, C. A.; Johnson, W. C. Circular Dichroism of the Nucleic Acid Monomers. *Biopolymers* **1977**, *16* (10), 2243–2264. https://doi.org/10.1002/bip.1977.360161012.

For Table of Contents Use Only